

The role of non-thermal electrons in the hydrogen and calcium lines of stellar flares

M. D. Ding and C. Fang

Department of Astronomy, Nanjing University, Nanjing 210093, China

Accepted 2001 ??????. Received 2001 ??????; in original form 2001 ??????

ABSTRACT

There is observational evidence showing that stellar and solar flares occur in a similar circumstance, although the former are usually much more energetic. It is expected that the bombardment by high energy electrons is one of the chief heating processes of the flaring atmosphere. In this paper we study how a precipitating electron beam can influence the line profiles of Ly α , H α , Ca II K and λ 8542. We use a model atmosphere of a dMe star and make non-LTE computations taking into account the non-thermal collisional rates due to the electron beam. The results show that the four lines can be enhanced to different extents. The relative enhancement increases with increasing formation height of the lines. Varying the energy flux of the electron beam has different effects on the four lines. The wings of Ly α and H α become increasingly broad with the beam flux; change of the Ca II K and λ 8542 lines, however, is most significant in the line centre. Varying the electron energy (i.e., the low-energy cut-off for a power law beam) has a great influence on the Ly α line, but little on the H α and Ca II lines. An electron beam of higher energy precipitates deeper, thus producing less enhancement of the Ly α line. The Ly α /H α flux ratio is thus sensitive to the electron energy.

Key words: line: profiles – stars: activity – stars: atmospheres – stars: flare – stars: late-type.

1 INTRODUCTION

Stellar flares have been frequently detected in both broad band photometry and in spectral lines. A large stellar flare can be several orders of magnitude more energetic than its solar analogy. During a stellar flare, the continuum emission in UV and visible bands is significantly enhanced and is usually characterised by a blue colour (e.g. Pagano et al. 1997); on the other hand, spectral lines show an increased net emission, with a magnitude varying from line to line (e.g. Catalano & Frasca 1994; Montes et al. 1996); lines show asymmetries and macroscopic velocity fields of several hundreds of km s⁻¹ possibly exist (e.g. Houdebine et al. 1993; Gunn et al. 1994; Montes et al. 1999), implying that the flaring atmosphere is very dynamic.

A detailed comparison between stellar and solar flares was made by Haisch, Strong & Rodonò (1991). Despite the big difference in magnitude and scale, stellar and solar flares still show many similar features in the enhancement of lines and continua, implying further that the basic heating processes and emission mechanisms are similar in these two phenomena. It is widely accepted that a solar flare occurs through the reconnection of magnetic fields, which releases a large amount of thermal energy and results in the accel-

eration of charged particles. Accelerated particles then precipitate downwards to heat the lower atmosphere, leading to a dynamic evolution of the atmosphere (chromospheric evaporation and condensation). Although there is no direct information on spatially resolved magnetic activity on stars like that observed on the Sun, some observations still show evidence that a stellar flare may result from the interaction between an old magnetic structure and a new emerging flux (Catalano & Frasca 1994). Simon, Linsky & Schiffer (1980) proposed a speculative scenario of major long-lived RS CVn flares in which the component stars have very large corotating flux tubes, which occasionally interact. Recently, Rubenstein & Schaefer (2000) proposed that superflares, which are newly detected on F–G main-sequence stars by Schaefer, King & Deliyannis (2000), are caused by magnetic reconnection between fields of the primary star and a close-in planet. In these cases, the basic flare mechanism is also magnetic reconnection.

Therefore, we can postulate that the eruption of a stellar flare involves the acceleration of charged particles which then bombard the lower atmosphere. This process not only provides direct heating through Coulomb collisions, producing the bulk mass motions as revealed in the observed spectra (e.g. Houdebine et al. 1993), but also yields non-thermal

arXiv:astro-ph/0105097v1 6 May 2001

collisional excitation and ionization of the ambient atoms. The latter increases the source function and thus enhances the line and continuum emission. This issue is important in the spectroscopy and, in particular, the atmospheric modelling of stellar flares. It is then desirable to have a quantitative assessment of the non-thermal effects on both the line and continuum emission. Numerical computations including the non-thermal effects have been done mostly for solar flares (e.g. Fang, Hénoux & Gan 1993; Hénoux, Fang & Gan 1995; Ding & Fang 1997; Ding & Schleicher 1997; Ding 1999; Fang, Hénoux & Ding 2000). Recently, Ding & Fang (2000) studied the role of non-thermal electrons in the optical continuum of stellar flares. They found that an electron beam with a large energy flux can produce a U -band brightening and a $U - B$ colour that are roughly comparable with the observed values of a typical large flare. This work investigates how the non-thermal electrons influence the lines of hydrogen (H I Ly α and H α) and the lines of ionized calcium (Ca II K and λ 8542) which are frequently used in the spectroscopy of stellar atmospheres (e.g. Hawley & Pettersen 1991; Panagi, Byrne & Houdebine 1991; Houdebine & Doyle 1994a, 1994b; Houdebine & Stempels 1997).

2 COMPUTATIONAL METHOD

When an electron beam precipitates downwards from the corona, the beam electrons collide elastically with the ambient electrons and protons, leading to a direct heating of the plasma; meanwhile, the beam electrons collide inelastically with the ambient atoms and produce a non-thermal excitation and ionization of the atoms. As in Ding & Fang (2000), we first evaluate the rate of energy deposition corresponding to the latter process, which reads

$$\Phi = \frac{1}{2}(1-\xi)n_{\text{H}}\Lambda'K(\delta-2)\frac{\mathcal{F}_1}{E_1^2}\left(\frac{N}{N_1}\right)^{-\frac{\delta}{2}}\int_0^{u_1}\frac{u^{\frac{\delta}{2}-1}du}{(1-u)^{\frac{2+\beta}{4+\beta}}}, \quad (1)$$

where ξ is the ionization degree of the ambient plasma, $K = 2\pi e^4$, Λ' the Coulomb logarithm for inelastic collisions. We assume a power law flux spectrum for the electron beam, characterised by a power index, δ , a low-energy cut-off, E_1 , and a total energy flux, \mathcal{F}_1 . N is the column density and N_1 is the depth penetrated by electrons of an energy E_1 , which is expressed as

$$N_1 = \frac{\mu_0 E_1^2}{(2 + \beta/2)\gamma K}, \quad (2)$$

where μ_0 is the cosine of the initial pitch angle, taken to be unity here. The expression for β and γ can be found in Emslie (1978). Moreover, in equation (1),

$$u_1 = \begin{cases} 1, & N > N_1, \\ N/N_1, & N < N_1. \end{cases} \quad (3)$$

We adopt an atomic model of four bound levels plus continuum for hydrogen and a model of five bound levels plus continuum for ionized calcium. The non-thermal excitation and ionization rates are computed as

$$C_{ij}^{\text{B}} \simeq a_{ij}\Phi/n_1, \quad (4)$$

where n_1 is the hydrogen ground level population. The coefficients a_{ij} are taken from Fang et al. (1993): in cgs units,

$a_{12} = 2.94 \times 10^{10}$, $a_{13} = 5.35 \times 10^9$, $a_{14} = 1.91 \times 10^9$ and $a_{1c} = 1.73 \times 10^{10}$ for H; $a_{14} = 2.38 \times 10^{10}$, $a_{15} = 4.25 \times 10^{10}$ and $a_{1c} = 4.69 \times 10^{10}$ for Ca II. The above formulae for non-thermal collisional rates are derived empirically using the collisional cross-sections for various transitions (Fang et al. 1993). It is very convenient to include these rates into the computation of model atmospheres.

We do non-LTE computations using a method similar to that described in Gan & Fang (1987) and Fang et al. (1993). The general procedure is as follows. Given a model atmosphere and a prescribed electron beam, we solve iteratively the equations of hydrostatic equilibrium, particle conservation, radiative transfer and statistical equilibrium, including the non-thermal collisional rates (C_{ij}^{B}), for both H and Ca II. After the computations reach convergence, we then calculate the line source function and the opacity, and finally the line profile as

$$F_{\lambda} = 2\pi \int_0^1 I_{\lambda}(\mu)\mu d\mu = 2\pi \int_0^1 d\mu \int_0^{\infty} S_{\lambda}e^{-\tau_{\lambda}/\mu} d\tau_{\lambda}. \quad (5)$$

Broadening mechanisms include radiative damping, the Doppler effect and the Stark effect. Note that for all the lines involved, we assume complete frequency redistribution (CRD), while the effect of partial frequency redistribution (PRD) may be important for some lines (e.g. Ly α and Ca II K). However, CRD is still a reasonable assumption in the present investigation since our main purpose is to show the effect of non-thermal electron beams, not to reproduce exactly the observed line profiles.

3 INFLUENCE OF ELECTRON BEAMS ON THE LINE EMISSION

Many authors have investigated how the spectral lines, including the H I Ly α and H α , and the Ca II K and λ 8542 lines, change with the modifications of atmospheric models of, for example, late-type stars (e.g. Linsky et al. 1979; Houdebine & Doyle 1994a, 1994b; Houdebine, Doyle, & Kościelicki 1995; Houdebine & Stempels 1997; Short & Doyle 1997, 1998; Mauas 2000). These lines are shown to be good diagnostics of the atmospheric conditions in the late-type stars. Generally speaking, the Ca II K line, in particular, the K1 minimum, can be used to determine the temperature structure around the temperature minimum region; emission in the hydrogen Balmer lines (H α etc.) is related to the temperature and temperature gradient in the chromosphere; the Ly α flux relies sensitively on the position of the transition region, i.e., the coronal pressure. However, we will show below that the presence of a non-thermal electron beam in a flare star can also change these spectral features without modifying the atmospheric model. Therefore, in order to construct reliable semi-empirical models or make proper spectral diagnostics for these flare stars, we need first to study quantitatively the effect of non-thermal electrons on the above-mentioned lines.

3.1 Effect of varying the beam flux

As in Ding & Fang (2000), we adopt the semi-empirical model of the dMe star, AD Leo, proposed by Mauas & Falchi (1994), as the base model, and then introduce an

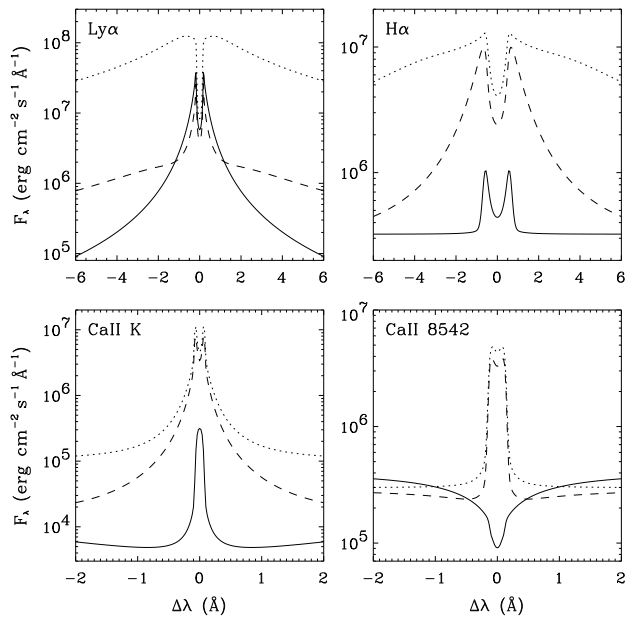


Figure 1. Line profiles of Ly α , H α , Ca II K and λ 8542 computed from a model atmosphere of the dMe star AD Leo (Mauas & Falchi 1994), considering the effect of a precipitating non-thermal electron beam. Different line styles show the effect of varying the energy flux, \mathcal{F}_1 , of the beam: 0 (solid line), 10^{10} (dashed line) and 10^{12} (dotted line) $\text{erg cm}^{-2} \text{s}^{-1}$. In all cases, the low-energy cut-off, E_1 , is 20 keV, and the power index, δ , is 3.

electron beam into the atmosphere to compute the emergent line profiles. We fix the model atmosphere by only changing the energy flux of the beam, covering a range of 10^9 – 10^{12} $\text{erg cm}^{-2} \text{s}^{-1}$, which are typical values for a solar flare case. Fig. 1 displays the four line profiles in different cases of beam fluxes. Generally speaking, the four lines undergo a drastic change when the beam flux increases. However, there is clearly a difference in the evolutionary behaviour of these lines. When the beam is not so strong ($\mathcal{F}_1 \lesssim 10^{10}$ $\text{erg cm}^{-2} \text{s}^{-1}$), the Ly α line shows only an increased emission in its far wings, while the inner part, including the emission peaks and the line centre, is not increased but somehow decreased. When the beam flux further increases, the whole line is enhanced significantly, except for the line centre, which remains as weak as in the quiescent state. The H α line shows instead a monotonic increase in the whole profile with the beam flux. In the case of a strong beam ($\mathcal{F}_1 \sim 10^{12}$ $\text{erg cm}^{-2} \text{s}^{-1}$), both the H α and Ly α lines become very broad. Quite differently, change of the Ca II K and λ 8542 lines is most significant in the line centre. While the wings of the K line can also be enhanced to some extent, the wings of the λ 8542 line are slightly reduced by the non-thermal effects.

To show more quantitatively the variation of the lines, we plot in Fig. 2 the net integrated flux, ΔF , defined as the flux integrated over the whole line profile with the quiescent value subtracted, against the electron beam flux. The integration extends to $\Delta\lambda = \pm 6$ Å for Ly α and H α lines and to $\Delta\lambda = \pm 2$ Å for Ca II K and λ 8542 lines, respectively. It can be seen that the extent of line flux enhancement increases in the order of Ca II λ 8542, K, H α and Ly α . From line profile computations, we can find that this is just the order of line

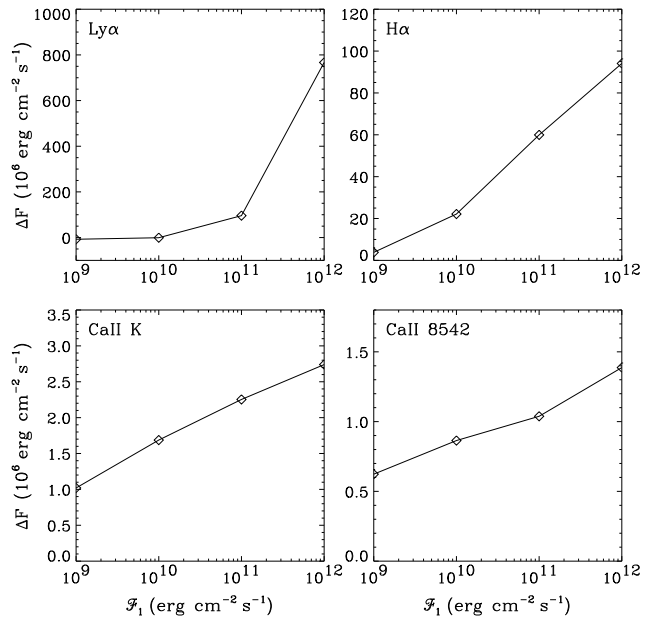


Figure 2. Net integrated fluxes of Ly α , H α , Ca II K and λ 8542 against the energy flux of the electron beam. In all cases, the low-energy cut-off, E_1 , is 20 keV, and the power index, δ , is 3.

formation heights, spanning a range from the upper photosphere or lower chromosphere to the upper chromosphere. So the results are compatible with the general picture that the electron beam precipitates downwards from the corona. We note that the negative value of ΔF for Ly α in weak beam cases is due to a reduction of emission in the inner part of the line, as described above.

3.2 Effect of varying the electron energy

To check the effect of non-thermal electrons of different energies, we have also computed the line spectra for electron beams with a fixed energy flux but different low-energy cut-offs. The line profiles and the net integrated fluxes are plotted in Figs. 3 and 4 respectively. Fig. 3 shows that, varying E_1 does not alter obviously the profiles of H α , Ca II K and λ 8542. However, it has a great influence on the Ly α profile, namely, increasing E_1 reduces the non-thermal effects on the line intensities. This result is not surprising. As the Ly α line is formed in the very upper chromosphere, electrons of a higher energy penetrate deeper and thus leave less energy in upper layers to excite the hydrogen atoms.

In the above computations, the electron beam is assumed to originate in the corona, i.e., at the top of the model atmosphere. If the beam originates in a lower layer, its effect could become more significant for lines formed in the lower atmosphere. Such a scenario has been proposed to be a possible origin of a flare-like phenomenon on the Sun, Ellerman bombs (Ding, Hénoux & Fang 1998).

3.3 Discussion

To illustrate the different behaviours of the four lines in response to the electron beam, we plot in Fig. 5 the height distribution of the line source function in different cases of

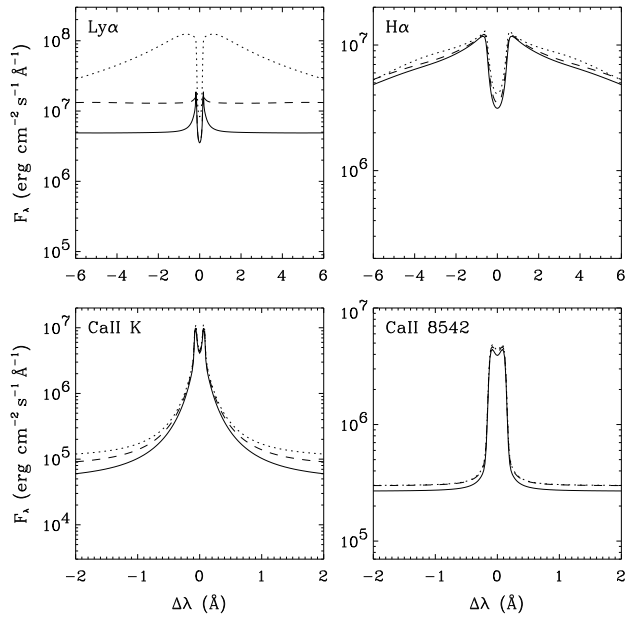


Figure 3. Line profiles of Ly α , H α , Ca II K and λ 8542 computed from a model atmosphere of the dMe star AD Leo (Mauas & Falchi 1994), considering the effect of a precipitating non-thermal electron beam. Different line styles show the effect of varying the low-energy cut-off, E_1 , of the beam: 20 (dotted line), 60 (dashed line) and 100 (solid line) keV. In all cases, the energy flux, \mathcal{F}_1 , is 10^{12} erg cm $^{-2}$ s $^{-1}$, and the power index, δ , is 3.

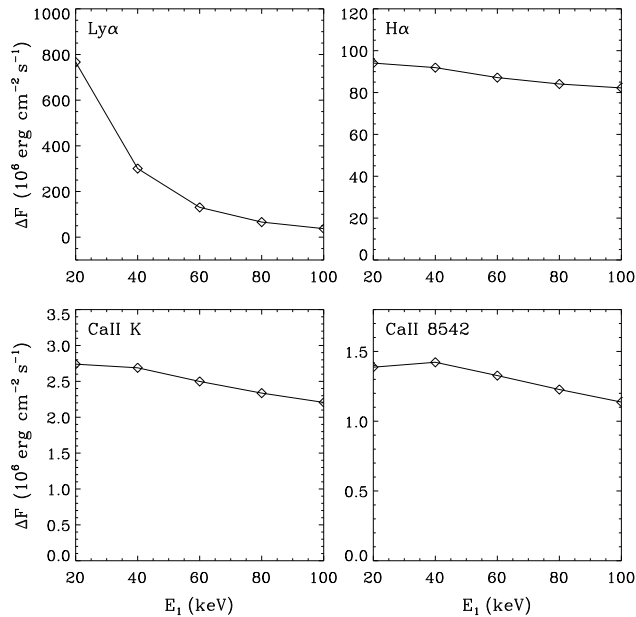


Figure 4. Net integrated fluxes of Ly α , H α , Ca II K and λ 8542 against the low-energy cut-off of the electron beam. In all cases, the energy flux, \mathcal{F}_1 , is 10^{12} erg cm $^{-2}$ s $^{-1}$, and the power index, δ , is 3.

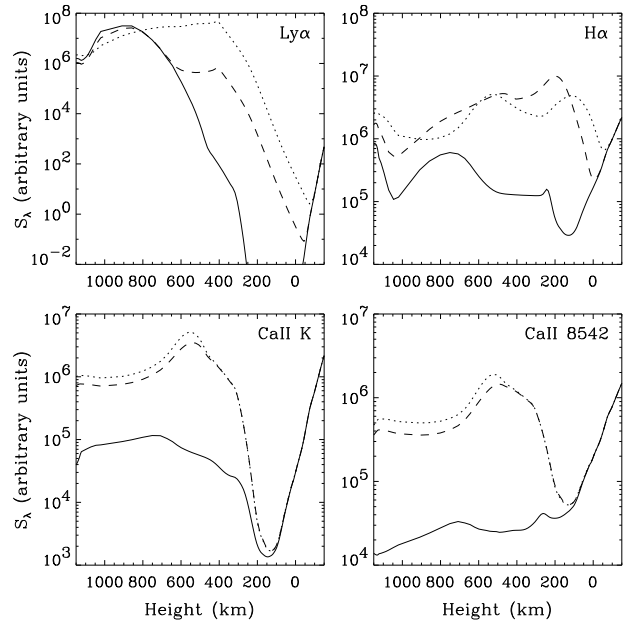


Figure 5. Height distribution of the source function of the four lines in the atmosphere of AD Leo in the presence of an electron beam. The line styles have the same meaning as in Fig. 1.

beam fluxes. It shows that the beam can make the source function of Ly α greatly increased in a broad region from the chromosphere to the photosphere. This can be understood that the hydrogen ground level is depopulated while the excited levels are overpopulated with respect to the beam-free case. Accordingly, the Ly α wings are significantly enhanced. In the very upper layers, however, the source function of Ly α could be slightly reduced, which results in a decrease of the line centre intensity in some cases (see Fig. 1). Similar results have been obtained for the Ly α line in solar flares (Hénoux et al. 1995). The source function of H α is also increased but less significantly than Ly α . Note that the Stark effect, due to an enhanced electron density, plays an important role in the broadening of the H α line. Fig. 6 displays the height distribution of the electron density, which is shown to be raised by up to three orders of magnitude in the chromosphere, highlighting the non-thermal ionization effect of the beam.

The increase of the source function of hydrogen lines in photospheric layers is mainly caused by a backwarming effect, i.e., the enhanced radiation from the chromosphere, while the direct penetration of non-thermal electrons has less effect. In contrast, the source function of the Ca II lines is mainly increased in the chromosphere; it is still coupled to the local Planck function in the photosphere. In addition, the Ca II lines are less affected by the Stark effect. Therefore, the enhancement of these lines is most apparent in the line centre, as shown in Fig. 1.

The quantitative results of line and continuum enhancement due to an electron beam are certainly model-dependent. In all the above computations, we have assumed a cool background atmosphere. In fact, the model atmosphere should change with the activity level of the star, especially when flare occurs. A model of the flaring state of AD Leo, for example, was proposed by Mauas & Falchi (1996).

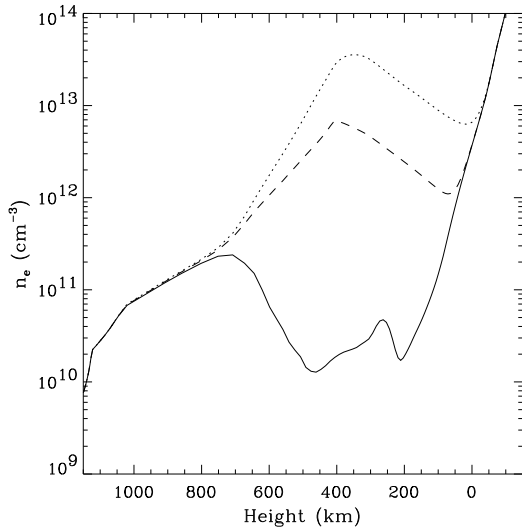


Figure 6. Height distribution of the electron density in the atmosphere of AD Leo in the presence of an electron beam. The line styles have the same meaning as in Fig. 1.

Compared with the model in the quiescent state, a flare model has a higher temperature in the chromosphere and even in the photosphere, and a lower position of the transition region (a higher coronal pressure). This model itself can produce an enhanced line emission. However, a higher coronal mass in the flaring atmosphere would consume a part of the electron energy, so that the effect of the electron beam is less significant than in the case of a quiescent atmosphere. The real situation might be a combination of the effects of a heated atmosphere and a non-thermal electron beam.

In addition to the line flux, we find that the $\text{Ly}\alpha/\text{H}\alpha$ flux ratio is in positive dependence on the electron beam flux, but, apparently, in negative dependence on the low-energy cut-off. In the case of $\mathcal{F}_1 = 10^{12} \text{ erg cm}^{-2} \text{ s}^{-1}$, $E_1 = 20 \text{ keV}$ and $\delta = 3$, the ratio amounts to ~ 6 . Therefore, it seems that an electron beam can produce most spectral features that are usually ascribed to a modification of the model atmosphere. As long as the electron beam exists during the flaring process, its effect should be taken into account in order to properly construct the semi-empirical models, otherwise the chromospheric temperature will be overestimated.

4 CONCLUSIONS

There is observational evidence showing that a stellar flare may occur in a similar circumstance to the eruption of a solar flare. A common flare scenario is the reconnection of magnetic fields. Although a stellar flare, in particular, the flares in late-type stars, can be several orders of magnitude more energetic than a solar flare, their emission features, in both lines and continua, still share many similarities. It can be postulated that the flaring process in a star also involves the acceleration of energetic particles (protons or electrons), carrying most energy to heat the lower atmosphere.

We study in this paper how a precipitating electron beam can influence the line profiles of $\text{Ly}\alpha$, $\text{H}\alpha$, Ca II K and $\lambda 8542$. We make non-LTE computations taking into ac-

count the non-thermal collisional rates due to the electron beam. The results show that the four lines can be enhanced to different extents. The relative enhancement increases with increasing formation height of the lines. Varying the energy flux of the electron beam has different effects on the four lines. The wings of $\text{Ly}\alpha$ and $\text{H}\alpha$ become increasingly broad with the beam flux; change of the Ca II K and $\lambda 8542$ lines, however, is most significant in the line centre. Varying the electron energy (i.e., the low-energy cut-off for a power law beam) has a great influence on the $\text{Ly}\alpha$ line, but little on the $\text{H}\alpha$ and Ca II lines. An electron beam of higher energy precipitates deeper, thus producing less enhancement of the $\text{Ly}\alpha$ line. The $\text{Ly}\alpha/\text{H}\alpha$ flux ratio is thus sensitive to the electron energy. Together with our computations for the continuum emission (Ding & Fang 2000), these results provide a diagnostic tool for the non-thermal processes in stellar flares.

ACKNOWLEDGEMENTS

We would like to thank the referee for his/her valuable comments on the manuscript. This work was supported by TRAPOYT, National Natural Science Foundation of China under grant 10025315 and National Basic Research Priorities Programme under grant G2000078402.

REFERENCES

- Catalano S., Frasca A., 1994, *A&A*, 287, 575
 Ding M. D., 1999, *A&A*, 351, 368
 Ding M. D., Fang C., 1997, *A&A*, 318, L17
 Ding M. D., Fang C., 2000, *MNRAS*, 317, 867
 Ding M. D., Hénoux J.-C., Fang C., 1998, *A&A*, 332, 761
 Ding M. D., Schleicher H., 1997, *A&A*, 322, 674
 Emslie A. G., 1978, *ApJ*, 224, 241
 Fang C., Hénoux J.-C., Ding M. D., 2000, *A&A*, 360, 702
 Fang C., Hénoux J.-C., Gan W. Q., 1993, *A&A*, 274, 917
 Gan W. Q., Fang C., 1987, *Chinese Astron. Astrophys.*, 11, 49
 Gunn A. G., Doyle J. G., Mathioudakis M., Houdebine E. R., Avgoloupis S., 1994, *A&A*, 285, 489
 Haisch B., Strong K. T., Rodonò M., 1991, *ARA&A*, 29, 275
 Hawley S. L., Pettersen B. R., 1991, *ApJ*, 378, 725
 Hénoux J.-C., Fang C., Gan W. Q., 1995, *A&A*, 297, 574
 Houdebine E. R., Doyle J. G., 1994a, *A&A*, 289, 169
 Houdebine E. R., Doyle J. G., 1994b, *A&A*, 289, 185
 Houdebine E. R., Doyle J. G., Kościelicki M., 1995, *A&A*, 294, 773
 Houdebine E. R., Foing B. H., Doyle J. G., Rodonò M., 1993, *A&A*, 274, 245
 Houdebine E. R., Stempels H. C., 1997, *A&A*, 326, 1143
 Linsky J. L., Hunten D. M., Sowell R., Glackin D. L., Kelch W. L., 1979, *ApJS*, 41, 481
 Mauas P. J. D., 2000, *ApJ*, 539, 858
 Mauas P. J. D., Falchi A., 1994, *A&A*, 281, 129
 Mauas P. J. D., Falchi A., 1996, *A&A*, 310, 245
 Montes D., Saar S. H., Collier Cameron A., Unruh Y. C., 1999, *MNRAS*, 305, 45
 Montes D., Sanz-Forcada J., Fernández-Figueroa M. J., Lorente R., 1996, *A&A*, 310, L29
 Pagano I., Ventura R., Rodonò M., Peres G., Micela G., 1997, *A&A*, 318, 467
 Panagi P. M., Byrne P. B., Houdebine E. R., 1991, *A&AS*, 90, 437
 Rubenstein E. P., Schaefer B. E., 2000, *ApJ*, 529, 1031
 Schaefer B. E., King J. R., Deliyannis C. P., 2000, *ApJ*, 529, 1026

Short C. I., Doyle J. G., 1997, A&A, 326, 287

Short C. I., Doyle J. G., 1998, A&A, 336, 613

Simon T., Linsky J. L., Schiffer F. H., III, 1980, ApJ, 239, 911